Alexander Balandin, *Phys. Low-Dim. Structures*., ½, 1 (2000).

Thermal Properties of Semiconductor Low-Dimensional Structures

Alexander Balandin
Department of Electrical Engineering
University of California – Riverside
Riverside, California 92521

ABSTRACT

In this paper we review our work on thermal and thermoelectric properties of semiconductor low-dimensional structures, e.g. quantum wells and quantum wires, with emphasis on the effects of spatial confinement of acoustic phonons. We particularly concentrate on calculation of the phonon relaxation rates in mass-difference, Umklapp, point defect, and dislocation scattering processes that takes into account confinement of phonon modes. A possibility of device performance enhancement via phonon engineering and thermoelectric applications of low-dimensional structures are also discussed.

I. Introduction

Thermal properties of semiconductor nanostructures and superlattices have recently attracted a lot of attention. This is primarily due to two major factors. The first one is a continuous scaling down of the feature sizes in microelectronic devices and circuits,

which leads to an increase in power dissipation per unit area of semiconductor chip. Under such conditions, the influence of size effects on thermal conductivity becomes extremely important for device design and reliability [1]. The problem of thermal management is even more severe for photonic devices such as vertical cavity surface emitting lasers in which the heat generation density reaches 10^6 W/cm^3. The second factor is a rebirth of the field of thermoelectric materials, which has been brought about by the emergence of large numbers of new artificially synthesized materials, including those structured on an atomic scale [2]. In order to dissipate the increasing amount of heat from the chip area, one has to engineer material parameters or structure geometry in such a way that thermal conductivity is large along particular directions. To improve performance of thermoelectrics, one needs to achieve low thermal conductivity. These are two contradictory demands, but both can be approached with appropriate modification of phonon modes, e.g. *phonon engineering*.

It was shown earlier that phonon transport in superlattices can be significantly modified due to formation of minibands and emergence of the mini-Umklapp process, a new type of the Umklapp scattering processes associated with transitions between the mini-Brillouin zones [3]. A dramatic suppression of the perpendicular thermal transport in superlattices at high temperatures was also predicted in Ref. [4]. In the structures considered in Ref. [3], the modification of phonon transport comes from the periodicity (additional to the crystal lattice periodicity) in the direction of superlattice layering. In such a case, the mini-reciprocal lattice vectors associated with superlattice minizones give rise to mini-Umklapp processes which contribute to the thermal resistance. The situation is quit different in single quantum wells, which are either free-standing or embedded into material with distinctively different elastic properties. Here, the phonon dispersion changes due to the phonon spatial confinement induced by the boundaries. In this review, we address the issue of how spatial confinement of acoustic phonon modes directly modifies the lateral lattice thermal conductivity of quantum wells and quantum wires with rigid or free-surface boundaries.

Recently, several groups reported the results of experimental investigation of the lateral thermal conductivity k_{ph} of thin films [5,6]. In all cases the strong drop was observed. Zheng *at al.* [5] carried out measurements using a suspended micro structure, and found an extremely large reduction of k_{ph} (more than an order of magnitude) in the temperature range from T= 293 K to T=413 K. Such a huge drop in thermal conductivity can not be attributed entirely to boundary scattering and structure imperfections, and is likely related to modification of phonon modes and corresponding change in the thermal transport. Geometry of a quantum well structure, material parameters and temperature regime used in the theoretical models presented here approximately correspond to the conditions of the experiments.

The development of sophisticated pattering and self-assembly techniques for quasi one-dimensional (1D) semiconductor structures (quantum wires) [7-8] has stimulated a large body of new work in semiconductor physics over the last ten years. Quantum wires with widths down to 10 nm and small size fluctuations have been fabricated by regular electron beam lithography and wet etching [9]. Much of this interest to quantum wires was further stimulated by the possibility of novel "low dimensional" physics related to spatial confinement of carriers and phonons [10-11], as well as applications in electronic and optoelectronic devices. It has also been suggested that the thermoelectric figure of merit $ZT=S^2\sigma/(k_{ph} + k_e)$ can be significantly enhanced in quantum wells [12] and quantum wires [13] because of strong carrier confinement (where S is the Seebeck coefficient, σ is the electric conductivity, k_{ph} is the lattice thermal conductivity, and k_e is the electronic thermal conductivity). An increase to the thermoelectric figure of merit may also come from the drop of the lattice thermal conductivity in low-dimensional structures due to the increased phonon-boundary scattering [14]. Experimental evidence of the thermal conductivity drop in thin Si films has also been demonstrated [15]. Most recently Balandin and Wang [16] and Khitun *et al*. [17] have shown that an additional increase to ZT can be brought by the spatial confinement of acoustic phonons in thin films (quantum wells) [16] and quantum wire structures [17] embedded within material of distinctively different elastic properties. Thus, low-dimensional confinement of both carriers and phonons allows for more degrees of freedom in maximizing ZT.

The experimentally observed increase of the Seebeck coefficient in SiGe/Si multiple-quantum well structures has already given a confirmation of the advantages of low dimensionality [18]. To date, most of the experimental attempts to attain increased thermoelectric characteristics in low-dimensional structures were carried out with semiconductor superlattices or multiple-quantum well structures. Utilization of quantum wires for thermoelectric applications would require a two-dimensional array of quantum wires fabricated using e-beam lithography or self-assembly techniques. Difficulties of high-quality fabrication of such an array explain the scarcity of the experimental data for quantum wires. As a prototype system for theoretical study of thermal conductivity we have chosen silicon quantum wires. This choice was made for two reasons. Firstly, Si/Ge material system (in its bulk or nanostructured form) has already shown a great promise for high-temperature thermoelectric applications. Secondly, the problem of lattices thermal conductivity in silicon quantum wires is also important in a view of continuous down scaling of the device feature size, which will lead to the increased heat dissipation per unit area. Further development of the deep-submicron technology and growing utilization of ultra-thin silicon-on-insulator (SOI) structures make the problem of heat management of nano-size structures particularly acute.

The paper is organized as follows. In the next two sections we describe calculation of the lattice thermal conductivity which takes into account modification of the acoustic phonon dispersion due to spatial confinement. The model is based on the proper modification of the corresponding bulk formulas and phonon group velocities obtained from the continuous medium approximation with specific boundary conditions. It also takes into account new selection rules for three-phonon Umklapp processes imposed by emergence of additional phonon dispersion branches. Discussion and comparison of the theoretical results with available experimental data are given in section IV. In sections V - VII, we present the theory of confined phonon transport in semiconductor quantum wires. Confinement of acoustic phonons and corresponding change in their group velocity lead to an increase in the phonon relaxation rates and, thus to the drop in thermal conductivity.

Section VIII presents a discussion of the possibility of enhancement of the thermoelectric figure of merit via phonon engineering. We give our conclusions in section IX.

II. Confined phonon transport in quantum wells

Thermal conductivity of semiconductors is the sum of the lattice (phonon) k_{ph} and electronic k_e components. The characteristic ratio of these two obtained for doped semiconductors is k_e/k_{ph} ~ ½. For intrinsic silicon structures this ration is even lower. Thus, for simplicity, in this review we will only discuss the lattice (phonon) contribution to the thermal conductivity and neglect its electronic part. We consider a generic quantum well structure (see Fig. 1) at relatively high temperatures so that three-phonon interaction is expected to be the dominant scattering mechanism limiting heat transfer. It is well known that the normal three-phonon scattering processes (N-processes) in which the total momentum is conserved cannot by themselves lead to a finite thermal resistance, although they influence it indirectly by redistributing phonon modes [19-20]. Only processes, which do not conserve crystal momentum, contribute to the lattice thermal resistance. Such processes, further referred as resistive, are boundary scattering, impurity scattering, and three-phonon Umklapp scattering process (U-process) in which the sum of phonon wave vectors is not conserved but changes by a reciprocal-lattice vector. Impurity scattering, in its turn, can be separated for isotope scattering arising from the presence of atoms with different mass dislocation scattering, and scattering on atoms of different elements. In a high quality material, all of these impurity scattering mechanisms can be strongly reduced except for the isotope scattering. Due to this reason, we will be primarily interested in examining the effects produced by phonon confinement on the resistive processes, which include the three-phonon Umklapp processes, isotope scattering, and boundary scattering.

The lattice thermal conductivity can be written as [19-20]

$$k_{ph}=(1/3)\Sigma S(\omega)v_g\Lambda(\omega)d\omega, \quad (1)$$

where $S(\omega)$ is the contribution to the specific heat per frequency interval from phonons of frequency ω, $\Lambda(\omega)$ is the phonon mean-free-path (attenuation length), and v_g is the phonon group velocity. Using the relaxation-time methods the expression for k_{ph} we can be further rewritten as [20-22]

$$\kappa_{ph} = \frac{k_B}{2\pi^2 \upsilon_g} \left(\frac{k_B}{\hbar} \right)^3 T^3 \int_0^{\frac{\theta}{T}} \frac{\tau_C x^4 e^x}{\left(e^x - 1\right)^2} dx, \tag{2}$$

where $x = \hbar\omega/k_B T$, k_B is the Boltzmann constant, $\hbar$ is the Plank constant, θ is the Debye temperature, τ_C is the combined relaxation time, and υ_g is the phonon group velocity. The above equation for thermal conductivity is valid under the assumption that the resistive scattering mechanisms, which do not conserve crystal momentum, are dominant [19]. These are the processes that contribute to the lattice thermal resistance. The general expression for the lattice thermal conductivity, which includes an additional term for the normal scattering processes, can be found in Ref. [19-20].

The combine scattering relaxation time is found from Matthiessen's rule

$$\frac{1}{\tau_C} = \frac{1}{\tau_U} + \frac{1}{\tau_B} + \frac{1}{\tau_M} + \frac{1}{\tau_R}, \tag{3}$$

where τ_C is the combined phonon relaxation time due to different scattering mechanisms which are dominant in silicon at room temperature and above. Particularly, the mechanisms include Umklapp scattering (τ_U), boundary scattering (τ_B), mass-difference (or isotope) scattering (τ_M) and resonant scattering (τ_R) for a silicon with a high concentration of impurity atoms. In order to determine the lattice thermal conductivity, we calculate all phonon relaxation times in a low-dimensional structure taking into account their modification due to spatial confinement of phonon modes. Mass-difference scattering arises due to the presence of atoms with a mass different from the average atomic mass in a semiconductor. Different mass can come from the isotopes of particular elements or impurity atoms. In the latter case, the difference in stiffness constants

between the impurity-host atoms and the host-host atoms, as well as the difference in the atomic volume of the impurity atoms should also be included in the phonon scattering rate expression. We use the standard formula for the mass-difference scattering but introduce one important modification – group velocity dependence on the structure geometry and boundary conditions. The mass-difference scattering rate is written as [19-20]

$$\frac{1}{\tau_M} = \frac{V_0 \omega^4}{4\pi \upsilon_g^3} \Gamma_M \ , \tag{4}$$

where V_0 is the volume per atom, ω is the phonon frequency. The form-factor Γ_M depends on fraction of impurities in the host material, as well as mass, volume, and stiffness constant difference between the host atom and the impurity (isotope) atom. The exact expression and numeric values can be found in Ref. [17]. Phonon confinement effects enter the equation for the mass-difference scattering rate through modification of the phonon group velocity, which has to be calculated for each particular geometry and boundary conditions [16, 23, 24]. Since in nature silicon always contains a mixture of three main isotopes (92% of ^{28}Si, 4.6% of ^{29}Si, 3.1% of ^{30}Si), the isotope scattering significantly contributes to the thermal resistance of the material. The boundary scattering in this model is treated in the Casimir limit [25], with the phonon-boundary scattering rate presented as

$$\frac{1}{\tau_B} = \frac{v_g}{D} . \tag{5}$$

Resonance scattering is a process in which phonons interact with some localized modes. Under certain conditions, the impurities or point defects in a host semiconductor, which have some internal frequency of oscillation ω_0, can give rise to the resonance absorption on this resonance frequency [26]

$$\frac{1}{\tau_R} = \frac{R\,\omega^2}{\left(\omega_0^2 - \omega^2\right)^2 + \Omega\,\omega_0^2 \omega^2} , \tag{6}$$

where R depends upon the concentration of the impurities (point defects) and Ω is related to damping. We will illustrate the resonant scattering effects using the silicon - germanium materials system as an example in section VII when we will consider high concentration of Ge impurities. In this section we assume intrinsic Si quantum well, and disregard the resonance frequency term. The single-mode relaxation rate of the U-process for a thermal mode q have been derived by Klemens using the first-order perturbation theory [20-21]. Since the equations are rather complicated, they are not reproduced here. Phonon confinement effects enter the relaxation rates in the U-process via modification of the phonon group velocity and mode selection rules [16].

In order to evaluate relaxation rates for all the above processes, one should use the actual dispersion relations and group velocities, $v_g = v_g(\omega(q))$, for phonons in a quantum well. The modification of wave vector selection and frequency conservation rules due to the *spatial confinement* should also be taken into account. Evaluation of the single-mode relaxation rate of the mode q, requires the integration over all possible q modes. The outline of the method to calculate dispersion of confined phonons and their group velocity is given in the next section. Details of the calculation of $v_g = v_g(\omega(q))$, and $1/\tau_U$ have been presented in Ref. [16].

III. Phonon dispersion and group velocities in quantum wells

Most of the heat in silicon at room temperature or above is carried by the acoustic phonons with the wave vectors q close to the center of the Brillouin zone. In this region of the q-vector space, we can determine the phonon dispersion in the elastic continuum approximation. In order to calculate the phonon dispersion and phonon group velocities one has to solve the elasticity equation using the regular approach outlined in Ref. [27-29]. The elasticity equation is written in a vector form as follows

$$\frac{\partial^2 u}{\partial t^2} = s_t^2 \nabla^2 u + (s_l^2 - s_t^2)\Delta u \tag{7}$$

where $s_l = (\lambda + 2\ \mu)/\rho$ and $s_t = \mu / \rho$ are the velocities of longitudinal and transverse acoustic phonon modes in bulk semiconductors and λ, μ, ρ are Lame constants and ρ is the density. For Si, s_l=9.04 x 10^5 cm/s and s_t=5.34 x10^5 cm/s. The normal components of the stress tensor on the free-standing quantum well must vanish. These boundary conditions bring about a significant change to the phonon dispersion and group velocities as compared to bulk. One should note here that a significant modification of phonon modes can be attained not only in a free-standing quantum well but also in a quantum well embedded in rigid material (Si_3N_4 and SiO_2 for example) or in any other heterostructure with relatively large difference of elastic properties. In the case of a quantum well embedded in rigid material, the normal components of the stress tensor are unrestricted but the displacement $\boldsymbol{u}$ is zero at the boundary. This corresponds to the clamped-surface boundary conditions [27].

There are three different types of confined acoustic modes in a quantum well characterized by their distinctive symmetries [27]: shear (S) waves, dilatational (D) waves, and flexural (F) waves. The S modes are similar to the transverse (T) modes in bulk semiconductor and have only one non-zero component of the displacement vector $\boldsymbol{u}=(0, u_y, 0)$ which is perpendicular to the direction of wave propagation, $\boldsymbol{q}_{//}=(q_x,0)$, and lies in the plane of the quantum well. The dispersion relation for the S modes can be written as $\omega_n=s_t(q_x^2+ q_{z,n}^2)^{1/2}$, where subscript n denotes different branches of the same polarization type, and the $q_{z,n}$ is quantized as $q_{z,n}=\pi n/W$. The D and F phonon modes have two non-zero components $\boldsymbol{u}=(u_x, 0, u_z)$ with dispersion relation given by $\omega_n=s_l(q_x^2+q_l^2)^{1/2}$ where the set of parameters q_l defines different branches of the same polarization denoted by subscript l. Since these types of confined waves have a component in the direction of propagation, they can be viewed as a modification of the bulk longitudinal (L) mode.

Solving numerically the elasticity equation, one can find confined phonon modes for a particular well width and material parameters and then, by numerical differentiation, determine the group velocities. The phonon group velocity in the n branch is defined as $v_g(\omega)= d\omega_n/dq$. The dispersion relation for the phonons of D and S modes for a 10 nm wide Si quantum well are shown in Fig. 2 and Fig. 3, respectively. Corresponding group

velocities are the slopes of the phonon dispersion branches presented in Figs. 2 and 3. It is easy to see that there are more dispersion and velocity branches for each polarization type as compared to the bulk, and group velocities of all branches decrease. The higher the mode number the smaller the group velocity.

The change of polarization types and the $\omega(q)$ dependence brings also modifications of the energy and momentum conservation laws [23]. It is known that for isotropic semiconductor only two general types of processes are allowed: T+T ←→ L, or L+T ←→ L. This restriction follows from the requirement that (i) all three interacting modes cannot belong to the same polarization branch, and (ii) the resultant mode should be above two initial (interacting) modes. It turns out that for confined acoustic phonons, the D mode is almost always above the S mode corresponding to the same branch *n*. Comparing dispersion for S and D modes for a 10 nm wide Si quantum well, one can see that only for a small fraction of phonons with in-plane wave vectors close to the zone center, some branches of the D mode may have a smaller energy than that of the corresponding S mode [16]. Thus, the processes D_n+S_n ←→ D_n and S_n+S_n ←→ D_n are allowed and can be treated by analogy with the bulk processes or L+T ←→ L and T+T ←→ L, respectively. In this model calculations we have neglected the S and D mode intermixing close to the zone-center. More precise treatment would require separation of the frequency range where the S mode is higher in energy than the D mode, and considering D_n+S_n ←→ S_n as an allowed process. Details of the calculation procedure for U-processes have been reported by Balandin and Wang [16]. In their numerical calculations they have neglected optical phonon modes since for Si, particularly in *<110>* direction, their contribution in thermal transport is less significant than that one of the confined acoustic phonon modes. Although, for some material systems (like LiF or NaF), the optical dispersion curve intercepts all longitudinal bulk modes in all directions - *<100>, <110>, <111>* - and thus has to be included. Since optical phonon modes are not significantly affected by spatial confinement, the situation in quantum wells is not expected to be different from the bulk.

Finally, the phonon scattering rates have been evaluated for a bulk Si 10 μm thick slab (bulk) and Si 10 nm and 155 nm wide quantum wells. The material parameters used in simulation were the following: the lattice parameter a=5.45 A, density ρ=2.42 x 10^3 kg/m^3, mass of an atom M=46.6 x 10^{-27} kg, the number of atoms per unit cell n_a ~ 7.3, Gruneisen parameter γ=0.56, θ=625 K, and the isotope factor Γ x 10^4 = 2.64 for three Si isotopes. In the case of bulk material, the U-process is a dominant scattering mechanism over almost the entire phonon frequency range, which is important for Si from 1.8 x 10^{13} rad/sec to 6.06 x 10^{13} rad/sec. The latter is expected at room temperature and above. The scattering rate due to boundaries is two orders of magnitude smaller then intrinsic scattering rates for a given slab thickness (bulk material). For a quantum well, the impurity scattering rate which is proportional to ω^4 takes the lead at phonon frequencies above 2.5 x 10^{13} rad/sec. The dominant mechanism at low phonon frequencies is the boundary scattering. The overall scattering rate increases in a quantum well. One important thing to note is that by improving crystal and surface quality one can reduce the impurity and boundary scattering rates but not the Umklapp scattering rate. The increase of the U-process scattering rate in a quantum well is a direct result of the modification of phonon dispersion due to spatial confinement of the phonon modes. The later leads to the reduction of the group velocity which also strongly increases the impurity scattering as it is proportional to $1/v_g^3$.

IV. Comparison of thermal conductivity of silicon quantum wells and bulk

Fig. 4 presents the lattice thermal conductivity as a function of the temperature for the quantum well and the bulk material. In order to illustrate the contributions of different scattering mechanisms to the thermal resistivity, the conductivities limited only by the Umklapp scattering and by the Umklapp and impurity scattering are also shown. The Umklapp limited conductivity drops about 3.5 times because of the spatial confinement of phonons. The overall thermal conductivity of a quantum well at 300 K is about 13% of the bulk Si. The calculated value of the thermal conductivity and its temperature dependence are consistent with the results of the experimental investigation recently

reported by Zheng *et al.* [5]. The measurements reported in Ref. [5] have been conducted with a suspended micro-structure which served as a thermal bridge using the differential and equivalent circuit methods. These measurements have shown that the lateral thermal conductivity of a Si_3N_4 (150 nm) / monocrystalline Si (155 nm) / SiO_2 (300 nm) structure was about 1.5% of the conductivity of the bulk Si and was almost a constant in the temperature range from T=293 K to T=413 K. The total error for the measurements was estimated to be less than 20 %. Although the model presented here assumed a free-standing quantum well, the results can be extended to quantum wells with rigid boundaries. The lowest confined phonon modes in quantum well with clamped-surface boundary conditions are higher in energy than those in a free-standing quantum well, but the overall behavior and the decrease of the group velocities are very similar in both cases. This will be shown in details in section VI. The model presented here can be developed further to include mixed boundary conditions and interface quality. Applied to a 155 nm wide Si well, this model gives k_{ph}=66.7 W/mK. For comparison, experimentally measured thermal conductivity of bulk Si is 148 W/m K. This is a significant drop although much less then that observed in the experiment. The temperature dependence of the calculated k_{ph} is very close to the measured one. The discrepancy in the calculated and measured values of k_{ph} maybe attributed to (i) underestimated in the model boundary scattering, (ii) presence of other defect scattering processes (like scattering on dislocations), or (iii) crystal anisotropy, strain effects and related phonon focusing.

The theoretical results presented in this review are in a good agreement with the recent data reported in Ref. [31]. In Ref. [31], the authors predicted a significant reduction of the in-plane lattice thermal conductivity for Si layers thinner than 0.2 μm at temperatures as high as 700 K. In accordance with their model, the thermal conductivity of a 0.05 μm pure Si film at 400 K in silicon-on-insulator structures is about 30 % of the bulk value. Further reduction of the layer thickness and inclusion of the phonon confinement effect would lead to much stronger decrease of the thermal conductivity. It was also reported there that the lattice thermal conductivity of the $Bi_{0.5}Sb_{1.5}Te_3$ films is considerably lower than that of bulk crystals of the same solid solution. The experimentally observed

temperature dependence in Ref. [32] is very close to the one calculated on the basis of our model.

V. Confined phonon transport in quantum wires

In this section we investigate the phonon transport and the lattices (phonon) thermal conductivity in a generic cylindrical silicon quantum wire taking into account modification of the acoustic phonon modes and phonon group velocities in free- and clamped-surface wires due to spatial confinement effects. At room temperature and above, acoustic phonons, with the wave vectors close to the Brillouin zone center, carry most of the heat in silicon bulk material and low-dimensional structures, including quantum wires. In order to calculate the thermal conductivity of quantum wires we use the same type of formalism as we used for quantum wells (thin films) in the previous section but substitute phonon dispersion and group velocity found for quasi-1D structures. The above equations for thermal conductivity and phonon scattering rates were initially derived for bulk semiconductors. We extended them to a low-dimensional structure assuming that a quantum wire has finite radius $r \gg a_o$, where a_o is the lattice constant. Phonon confinement effects enter these equations through modification of the phonon group velocity, which has to be calculated for each particular geometry and boundary conditions. In the limiting case of strictly one-dimensional (1D) structure the phonon frequency dependence in the equation for mass-difference scattering changes to $1/\tau_M \sim \omega^2$ [20]. We will not consider this case and limit our analysis to the realistic situation with wire diameter a ~ 20 nm or larger. Since in nature silicon always contains a mixture of three main isotopes (92% of ^{28}Si, 4.6% of ^{29}Si, 3.1% of ^{30}Si), the isotope scattering significantly contributes to the thermal resistance of the material. The boundary scattering in our model is again treated in the Casimir limit. It can be shown that the effective boundary mean-free-path $\Lambda(\omega)$ for a cylindrical quantum wire of diameter a in the Casimir limit is given by $L_o=a$ [25]. (For a rectangular quantum wire with a square cross section with side W, the Casimir limit mean free path is $L_o = 1.12W$). Thus, the

phonon-boundary scattering rate for a cylindrical quantum wire can also be calculated using the same formula as for the quantum well (see section II).

In order to evaluate phonon relaxation rates in quantum wires, one should use the actual dispersion relations and group velocities, $\upsilon_g \equiv \upsilon_g(\omega(q))$, for phonons in the free-surface and clamped-surface quantum wires. The modification of wave vector selection and frequency conservation rules due to the spatial confinement should also be taken into account while dealing with the Umklapp processes. The phonon dispersion and phonon group velocities are found from the elasticity equation. We consider a cylindrical wire of infinite length in the *z* direction and with a diameter *a* (see Fig.5). For simplicity it is assumed that the material of a wire has an isotropic symmetry and it does not have the azimuthal dependency. The components of the stress tensor are written as

$$\sigma_{zz} = \lambda\left(\frac{\partial u_r}{\partial r} + \frac{u_r}{r} + \frac{\partial u_z}{\partial z}\right) + 2\mu\frac{\partial u_r}{\partial r},$$

$$\sigma_{rz} = \mu\left(\frac{\partial u_r}{\partial z} + \frac{\partial u_z}{\partial r}\right). \tag{8}$$

We consider longitudinal and shear modes of the confined acoustic phonons because of their dominant contributions to the lattice heat transport. The analytical expressions for longitudinal acoustic waves, i.e. for displacements have been given in Ref. [29]. The displacements u_r and u_z are expressed through the ordinary Bessel functions J_0 and J_1, parameters q_l and q_t, some constants *A* and *B* (to be determined later), and the *z*-component wave vector (direction of propagation) *q*. Parameters q_l and q_t are related to the phonon frequency as

$$\omega = s_l\sqrt{q_x^2 + q_l^2} = s_t\sqrt{q_x^2 + q_t^2}, \tag{9}$$

The longitudinal waves are the coupled modes of the axial and radial modes that have the wave vectors q_l and q_t respectively. For share waves the displacement is given by a very simple expression

$$u_r(r,z) = J_1(q_t r)e^{i(qz-\omega t)}. \tag{10}$$

This phonon mode has only one non-zero component, which is perpendicular to the direction of wave propagation *(z)*. We will consider the both cases of boundary conditions: free-surface boundary, and clamped-surface boundary following the derivation of Khitun *et al* [17].

The free-surface boundary exactly corresponds to the boundary between an elastic material and vacuum, but can be used for a "rigid" material embedded within "softer" material. In this case the normal components of the stress tensor are vanish and the displacement is unrestricted: $\sigma_{z,z} = \sigma_{r,z} = 0$, at $r= \pm a/2$. The rigidity of the material can be quantitatively characterized by its characteristic phonon frequency $\Omega=(4F/M)^{1/2}$. Since $\Omega(Si)$ = 40.9 meV and $\Omega(Ge)$=22.9 meV, we can consider silicon wire embedded within germanium to have near-free surface boundary conditions. The ideal example of the free-surface silicon wire is the silicon whiskers grown by vapor-liquid-solid phase molecular beam epitaxy (MBE). The clamped-surface boundary conditions describe the case of the quantum wire made out of the "softer" material embedded within perfectly rigid material. In this case boundary conditions take the form $u_r = u_z = 0$, at $r= \pm a/2$.

Using the approach of Yu *et al* [29], one can obtain relations between q, q_l and q_t for longitudinal wave in the case of free- and clamped-surface boundaries. Resulting equations have many solutions for q_l and q_t (at each particular q), which are continuos single-connected curves "branches". We label them with an additional index n: $q_{l,n}$ and $q_{t,n}$. These solutions will be either real or pure imaginary depending on q and n. In our case, we are interested in the real part of solutions corresponding to the propagating phonon modes which carry the heat.

VI. Phonon dispersion and group velocities in quantum wires

Following Ref. [17], we numerically solving transcendental equations that determine acoustic phonon modes in quantum wires, and find confined phonon modes for particular wire material parameters and dimensions. Using calculated parameters q_l and q_t (real values only), we plot the dispersion relations (see Fig. 6) for the longitudinal modes for the free-surface (solid lines) and clamped-surface (dashed lines) boundaries. The diameter of the silicon quantum wire is again a=20 nm. The plot shows several branches of the lowest order. As the next step, the group velocity is obtained by the numerical differentiation. In order to determine the lattice thermal conductivity we have to find phonon group velocity as a function of phonon frequency. The functional dependence of the phonon energy and group velocity on the phonon wave vector is important for calculation of the Umklapp scattering rate. For evaluating the mass-difference scattering rates and boundary scattering rates, one needs to know the average phonon group velocity in the quantum wire. This velocity is expected to be different from that of the bulk. Different modes have different group velocities and the group velocity reaches the bulk sound velocity only in some specific very short energy intervals. In order to obtain resulting group velocity we take average group velocity as a function of phonon energy as follows,

$$\overline{\upsilon}_g(\hbar\omega) = \frac{\sum_n \upsilon_{g,n}(\hbar\omega) N_n(\omega)}{\sum_n N_n(\omega)} \tag{11}$$

where $\upsilon_{g,n}$ - group velocity of the nth mode, $N_n(\omega)$ - number of oscillators with frequency ω on the nth mode. The Boltzmann equation was used to find the relation for the density of oscillators between n^{th} and $(n+1)^{th}$ modes

$$\frac{N_{n+1}}{N_n} \approx e^{-(\hbar\omega)/k_B T} \tag{12}$$

The above equation is an approximation since we have a non-equidistant energy spacing for different phonon modes. The average group velocity obtained using this averaging procedure is depicted in Fig. 7 for Si and Ge quantum wires. Beginning with some phonon energy values the average group velocity coincides with the first mode group velocity, and then drops. The overall value of the average phonon group velocity is only about 1/2 of the bulk phonon group velocity (see Fig. 7). In a bulk the phonon group velocity approximately coincides with the sound velocity for small values of the phonon wave vector. This is a significant decrease.

After we found the average phonon group velocity over all contributing modes as a function of the phonon energy, we can obtain the lattice thermal conductivity using the equation in section I. The relaxation rates due to the different scattering mechanism are shown in Fig. 8 as functions of phonon frequency. In Fig. 8 we separated the mass-different scattering to the isotopic scattering, which is always present, and impurity (Ge) mass-different scattering. In the defect-free intrinsic bulk semiconductor the boundary, impurity (through mass difference) and resonant phonon scattering vanish. So that the thermal conductivity of the pure bulk silicon is determined only by the Umklapp and isotope scattering. The scattering processes become more complicated in the presence of many impurity atoms. One can see the strong influence of mass difference scattering on relaxation time in the presence of impurity with significantly different mass (as Ge with respect to Si). Beginning from early terahertz frequencies this different mass scattering became dominant. Resonance scattering mechanism can also lead to a significant increasing of relaxation time but it influence is localized in the vicinity of resonance frequency.

VII. Thermal conductivity of silicon quantum wires

In Fig. (9) we show the lattice thermal conductivity of a quantum wire as a function of temperature. The results are presented for the quantum wires with free- and clamped-surface boundaries as well as for the bulk material. The lattice thermal conductivity of the

quantum wires is less than 10% of the bulk silicon value in the temperature range from T=300K to T=700K. This significant decrease of the thermal conductivity is the result of the increased isotope, Umklapp, and boundary phonon scattering in a quantum wire. The latter comes from the modification of phonon dispersion due to spatial confinement. The change of the phonon modes leads to the reduction of the group velocity and, thus, increased phonon relaxation. Since the mass-difference scattering rate, which includes isotope scattering, is inversely proportional υ_g^3, even small decrease of the phonon group velocity gives rise to a strong increase in the phonon relaxation.

It is interesting to note that there is very little difference between thermal conductivity of a free-standing quantum wire (free-surface boundaries) and a quantum wire embedded within rigid material (clamped-surface boundaries). This means that the effect is always pronounced provided that (i) there is a *well-defined distinct boundary* between two materials of different elastic properties; and (ii) the lateral dimensions of the structure are small. The elastic properties can be characterized either by the characteristic phonon frequency (Ω(Si) =40.9 meV) or acoustic impedance $K = \rho v$, where ρ is the density, and v is the bulk sound velocity. The small difference in thermal conductivity drop for free-surface and clamed-surface boundaries can be explained as follows. Although different boundary conditions lead to the different phonon dispersion modes and different energy spacing between them, the slop of each dispersion mode, which defines the group velocity, is very close in both cases and is smaller than that in the bulk.

We also calculated the lattice thermal conductivity of Ge doped silicon quantum wires. As it was shown above, the lattice thermal conductivity is rather sensitive to the presence of the impurity atoms (via mass-difference scattering mechanism). It was found that 10% mole fraction of Ge can decrease silicon bulk thermal conductivity up to 10% of its initial bulk value. The experimental data point reported in Ref. [33] and our simulation data points are in good agreement [17]. One should mention that the combination of two factors, spatial confinement of phonons and presence of impurity atoms, can reduce the lattice thermal conductivity of a quantum wire up to few percent of the bulk value of its constituent materials. The decrease of the lattice thermal conductivity of an intrinsic

quantum wire obtained in our case is much more severe than the one recently reported in Ref. [34]. The authors in Ref. [34] treated in details the phonon-boundary scattering examining both diffusive and specular boundary scattering regimes. They found that the thermal conductivity drops five times (for a wire with 50 nm side) as compared to the bulk value. The decrease was attributed to the increased phonon-boundary scattering in the GaAs quantum wire. Although our results are qualitatively similar, we obtained stronger decrease of the thermal conductivity due to inclusion of phonon confinement effects. The discrepancy between these two-model descriptions is expected to be significant for narrow high-quality quantum wires embedded within material of different elastic properties. Under such conditions, the phonon modes are strongly confined and cannot be approximated with the regular bulk longitudinal and transverse modes [16]. Our data indicate that the decrease of the thermal conductivity in intrinsic free-standing quantum wires is larger than that which occurs in free-standing quantum wells of comparable size. Using the model for thermal conductivity of free-standing quantum well of Ref. [16], we found that at room temperature the following relation holds k_{ph}(wire)/k_{ph}(well) ~ 0.48. This value was obtained for a cylindrical silicon quantum wire of diameter a=20 nm and a rectangular silicon quantum well of thickness W=20 nm. The ration of the wire to well thermal conductivity obtained on the basis of our model is close to the one obtained in Ref. [34] although the model approaches are significantly different.

Decrease of the thermal conductivity revealed in this work and its mechanism are in qualitative agreement with some recent experimental findings for thin silicon films and Si/Ge superlattices. Liu *et al*. [35] have recently reported on the correlation between acoustic phonon folding in the small-period Si/Ge superlattices and the lattice thermal conductivity drop. It was found that the thermal conductivity of the superlattice with the period 33 A is 1.7 W/mK in the in-plane direction and 2.78 W/mK for the cross-plane direction, respectively. Obtained thermal conductivity was considerably lower than that determined using the bulk thermal conductivity values for Si, Ge, and Si_xGe_{1-x} alloys. This drop in thermal conductivity was attributed to the strong modification of the phonon modes and corresponding phonon velocities, which led to the phonon folding observed in Raman spectra [35]. A giant drop of the lattice thermal conductivity (more than an order

of magnitude) of the thin silicon film embedded within silicon nitride and silicon dioxide was reported by this group earlier [4]. Recent progress in fabrication of quantum wire arrays makes us to expect that such structures will soon be available for thermoelectric applications. One of the examples of such a structure is an array of Bi nanowires prepared using porous amorphous Al_2O_3 as a template [36]. The pores in amorphous Al_2O_3 are filled with Bi metal using a vacuum evaporation technique [36] or by the high-pressure liquid injection technique [37]. Another method of preparing quasi-periodic arrays of short nanowires of different materials using electrochemical deposition was reported in Ref. [38].

VIII. Thermoelectric figure of merit of quantum wires

Continuous progress in growth and self-assembly techniques for synthesizing quantum wires (quasi one-dimensional structures) [7] has stimulated a large body of work pertinent to these systems. Regular electron beam lithography and wet etching allow now to fabricate quantum wires with widths down to 100 A [9]. Clever techniques employing MBE growth of a narrow gap semiconductor on V-groove surfaces of a wider gap semiconductor have yielded quantum wires of unprecedented quality [39]. Carbon nanotubes are another example of quantum wires. The availability of such systems has resulted in a commensurately increased interest in their otoelectronic and thermoelectric properties.

Recently, there have been increasing number of studies on the modification of thermal conductivity [34] and the enhancement of the thermoelectric figure of merit $ZT=S^2\sigma T/k$ in quantum wires (S is the Seebeck coefficient, σ is the electrical conductivity, T is the absolute temperature, and $k=k_e+k_l$ is the sum of electron and lattice contributions to the thermal conductivity) [40, 41]. A large value of ZT (up to 14 at room temperature) was predicted for a Bi_2Te_3 quantum wire with width a=5 A [40]. The figure of merit of a quantum wire superlattice (a=20 A) was also shown to increase about 2.5 times from its bulk value of ZT_{3D}=0.53 [41]. In all cases the predicted increase came as a result of

carrier confinement and corresponding enhancement of the electron density of states near the Fermi level. The carrier mobility and lattice thermal conductivity were assumed to be equal to their corresponding bulk values [40-41].

More recently, Casian *et al*. [42] argued that decrease of the carrier mobility, which is expected in quantum wires of finite dimensions, may significantly offset the predicted increase of ZT in quasi one-dimensional structures. A strong drop in the electron (hole) mobility at room temperature in quantum wires of finite dimensions is explained by increased electron (hole) scattering on acoustic and optical phonons due to electron (hole) spatial confinement. Using the relaxation-time approximation, Sanders *et al*. [43] predicted decrease of the electron mobility in a Si quantum wire from 120 cm^2/Vs to less than 15 cm^2/Vs when the wire width decreases from 23 A to 10 A. This trend can only be reversed at low enough temperature when the elastic (impurity) scattering is a dominant scattering mechanism, and restriction of the phase space due to the spatial confinement leads to the mobility increase. The latter is a well-known Sakaki's result [44], which does not apply to the conditions of high-temperature thermoelectric applications of SiGe structures.

The studies on the thermoelectric figure of merit of quantum wires, reported in Refs. [40-42], had not included modification of the lattice thermal conductivity in quantum wires due to spatial confinement of phonons. This simplification is only valid for quantum wire structures with boundaries made out of material with similar crystalline and elastic properties such that phonon modes extend through the boundaries and do not differ significantly from the bulk. The situation is different for the quantum wires, which are either free-standing or embedded within material with distinctively different elastic properties (like Bi wires in alumina template). Here, phonon dispersion and group velocities are changed due to the spatial confinement induced by the boundaries. The phonon confinement affects all phonon relaxation rates, and makes the thermal transport properties of quantum wires rather different from those of bulk material in much the same way as in quantum wells (thin films) .

As an example system, we consider a $Si_{1-x}Ge_x$ quantum wire structure. The material system is chosen because of its bulk superior high-temperature thermoelectric properties. The mole fraction x of Ge is added to additionally decrease the lattice thermal conductivity, and to facilitate the integration of the quantum wires into a SiGe quantum wire superlattice. At the same time, the presented model will be applicable for other materials. Our model will use the derivations of the thermoelectric parameters for one-dimensional (1D) structures given by Hicks and Dresselhaus [40]. However, we do not assume that the lattice thermal conductivity k_{ph} equals to its bulk value. Rather, we calculate k_{ph} as a function of the wire radius a and temperature T.

Let us consider a quantum wire of circular cross-section that has a radius a and an infinite length along the x-axis. We assume that the wire has infinite potential barriers and only one occupied electron subband. The latter assumption is rather realistic for narrow wires with 1.5 nm < a < 15 nm. The energy spectrum for this wire can be written as [45]

$$E_{sn}(k_x) = E(k_x) + \frac{\hbar^2}{2m^*}(X_n^s / a)^2, \tag{13}$$

where s is the azimuth quantum number (s=0,±1,±2,...), n is the radial quantum number (n=1,2,3...), k_x is the axial electron wave vector, X_n^s is the nth zero of the Bessel function of the first kind, $E(k_x)$ is the electron kinetic energy along with the x direction, and m^* is the electron effective mass.

The general expressions of S, σ, k_e for bulk (3D), quantum well (2D), and quantum wire (1D) were derived using relaxation-time approximation [40,46]. In order to investigate the influence of the spatial confinement in a quantum wire on the ZT value, it is convenient to use the ratio between the wire and bulk parameters denoted by indices 1D and 3D respectively

$$\frac{S^{1D}}{S^{3D}} = \left(\frac{3F_{1/2}(\eta^{1D})}{F_{-1/2}(\eta^{1D})} - \eta^{1D}\right)\left(\frac{5F_{3/2}(\eta^{3D})}{3F_{1/2}(\eta^{3D})} - \eta^{3D}\right)^{-1}, \tag{14}$$

$$\frac{\sigma^{1D}}{\sigma^{3D}} = \frac{\pi\hbar^2}{a^2 k_B T (m_y m_z)^{1/2}} \frac{\mu_x^{1D}}{\mu_x^{3D}} \frac{F_{-1/2}(\eta^{1D})}{F_{1/2}(\eta^{3D})}, \tag{15}$$

where Fermi-Dirac function F_i is given by

$$F_i = F_i(\eta) = \int_0^\infty \frac{x^i dx}{e^{(x-\eta)}+1}, \tag{16}$$

with $\eta = \zeta / \kappa_B T$ being the reduced chemical potential (relative to the edge of the conduction band), T is the temperature, k_B is the Boltzmann constant, h is the Plank constant, m_x, m_y, m_z are the components of the effective-mass tensor, and μ_x is the mobility in the x direction. The reduced chemical potentials of the bulk and quantum wire are related as

$$\eta^{1D} = \eta^{3D} - \frac{\hbar^2}{2m^* k_B T}(X_n^s / a)^2. \tag{17}$$

For the fixed values of T and a, the reduced chemical potential depends on the doping level. The latter is used in order to maximize the ZT value. The ration of electronic contributions to thermal conductivity k_e^{1D}/ k_e^{3D} can also be expressed analytically via Fermi-Dirac functions [40, 46].

As we mentioned in the introduction, the reduction of the carrier mobility in a quantum wire of finite dimensions is caused by the spatial confinement of carriers. At room temperature, the dominant electron scattering processes are the longitudinal optical and acoustic phonon scattering processes [42,43]. In this work we use formulas derived in Ref. [42] under the assumption that spatial confinement of electrons does not significantly alter the electron-phonon scattering rates as it was shown by Nishiguchi [47]. At the same time, spatial confinement of phonons does change their Umklapp and point defects scattering rates [16], which will be included in the model when calculating the lattice thermal conductivity. It turns out that in a wide range of the quantum wire radii (from 10 A to 150 A), the acoustic phonon limited mobility is equal to the optical phonon

limited mobility. Casian *et al* [42] and Sanders *et al* [43] provide an integral equation for the ratio μ^{1D}/μ^{3D} expressed via modified Bessel function of the second kind K_1, the exponential integral function E_1, and parameter $l=h/m_x\omega_0$, where ω_0 is the limiting phonon frequency related to the Debye temperature. Another important factor, which was included in the present model, is the modification of the lattice thermal conductivity due to the spatial confinement of acoustic phonons [48]. It was shown by Balandin and Wang [16] that phonon modes within this region are subject to a significant modification in a quantum well structure, which leads to a strong drop in the lattice thermal conductivity. Khitun *et al* [48] have demonstrated that the phonon confinement effect is even stronger in quantum wires.

As it was already mentioned, Si_xGe_{1-x} material system was selected for numerical simulation for its great promise for high temperature thermoelectric applications. We have also already shown [48] that the lattice thermal conductivity of Si_xGe_{1-x} a quantum wire with clamped or free-surface boundaries experiences a huge drop, which makes its value equal to about 1% of the pure silicon bulk value. This drop is caused by the decrease of the phonon group velocity and corresponding increase in the phonon relaxation rates. The mass-difference scattering due to the presence of Ge atoms (m_{Ge}=3 m_{Si}) additionally contributes to the thermal conductivity decrease. We have chosen 10 % Ge content since it deteriorates the lattice thermal conductivity and at the same time does not dramatically reduce the electron mobility, which is about 50% of its pure Si value at this concentration. For numerical simulation, we assume that the x direction coincides with [100], so that $m_x = (2m_t + m_l)/3$, where $m_l = 0.9163 m_0$ and $m_t = 0.1907 m_0$ are the bulk longitudinal and transversal effective masses, respectively. For the first zero of $J_0(X)$ we take $s=0$, and $n=1$, and $X_1^0 = \sqrt{6}$. We also assume that $\theta = 625$K, and v_l = 8.47×10^5 cm/s, v_t =5.34×10^5 cm/s.

In Fig. 10 we depicted the carrier mobility and lattice thermal conductivity normalized to their bulk values as functions of the wire radius. One can see a significant decrease of both of these quantities, especially at the wire radii a<40 A. One should mention here, that the behavior of the mobility μ and the lattice thermal conductivity k_l are not directly

related. The decrease in μ comes about as a result of the increased electron-phonon scattering rates due to electron confinement, while the decrease of k_l is a result of the increased phonon relaxation due to phonon spatial confinement [10,11,16]. In principle, one can design a low-dimensional structure with strong phonon confinement but without electron confinement and vice versa. The structures where both electrons and phonons should be considered as spatially confined constitute one of the most interesting material systems currently being studied for thermoelectric applications [20,21].

As it is seen in Fig.10, *ZT* increases with decreasing wire radius but starts to saturate at the wire radius *a*=20 A. This saturation is caused by the sharp mobility decrease. It is interesting to note that despite the similar behavior of the *ZT* curve with the one presented in Ref. [40], the increase in *ZT* in our case *is mostly due to the decrease of the lattice thermal conductivity* rather than increased electron density of states [40,41]. The overall improvement of *ZT* came despite predicted decrease of the carrier mobility [42], which was included in our model.

IX. Conclusions

We have presented a review of some recent theoretical results on the thermal transport in low-dimensional structures such as quantum wells and quantum wires. Particular emphasis in this review has been on modification of acoustic phonon transport due to quantization of phonon modes and corresponding decrease of the lateral lattice thermal conductivity. It has been shown that strong modification of the phonon dispersion and group velocities due to spatial confinement leads to a significant increase of the phonon relaxation rates in three-phonon Umklapp scattering, impurity scattering, and isotope scattering processes, and as a result, to the decrease of the lattice thermal conductivity. The decrease is stronger in quantum wires than in quantum wells of corresponding dimensions and does not differ significantly for free-surface or clamped surface boundaries. Predicted decrease of the lattice thermal conductivity is important for further development of nanostructure-based thermoelectric devices. The decrease may also

complicate the heat management problem for future deep-submicron silicon-based devices and circuits. The theoretical results presented in this review favorably agree with the recent experimental investigation of the lateral thermal conductivity of quantum wells (thin films). It was shown that modification of the lattice thermal conductivity by confined phonon modes opens up a novel tuning capability of thermoelectric properties of heterostructures, and may lead to a strong increase of the thermoelectric figure of merit in specially designed semiconductor nanostructures.

Acknowledgements

The author acknowledges very helpful discussions on thermal conductivity with Prof. P.G. Klemens (University of Connecticut), Prof. Kang L. Wang (UCLA), and Prof. G. Chen (UCLA); as well as discussions on confined phonon transport in low-dimensional structures with Prof. S. Bandyopadhyay (University of Nebraska - Lincoln), Dr. A. Khitun (UCLA), and Prof. Fomin (University of Antwerpen).

Alexander Balandin, *Phys. Low-Dim. Structures*., ½, 1 (2000).

References

1. C.L. Tien, G. Chen, *ASME Journal of Heat Transfer*, **116**, 799 (1992).

2. F. J. DiSalvo, *Science*, **285**, 703 (1999); G. Mahan, B. Sales, J. Sharp, *Physics Today*, **50**, No.3, 42 (1997).

3. S.Y. Ren, J.D. Dow, *Phys. Rev. B*, **25**, 3750 (1982).

4. P. Hyldgaard, G.D. Mahan, *Phys. Rev. B*, **56**, 10754 (1997).

5. X.Y. Zheng, S.Z. Li, M. Chen and K.L.Wang, in *Micro-Electro-Mechanical Systems (MEMS)*, Proceedings of ASME International Mechanical Engineering Congress and Exposition (ASME, New York, 1996), pp.93-98.

6. Y.S. Ju and K.E. Goodson, *Appl. Phys. Lett*., **74**, 3005 (1999).

7. T. Kojima, J. Xue-Ying, Y. Hayafune, S. Tamura, *Japanese J. Appl. Phys. 1*, **37**, 5961 (1998).

8. V.S. Dneprovskii, E.A. Zhukov, E.A. Muljarov, S.G. Tikhodeev, *JETP*, **87**, 382 (1998).

9. A. Forchel, P. Ils, K.H. Wang, O. Schilling, *Microelectron. Engineer*, **32**, 317 (1996).

10. A. Svizhenko, A. Balandin, S. Bandyopadhyay, M.A. Stroscio, *Phys. Rev. B*, **57**, 4687 (1998).

11. V. M. Fomin, V. N. Gladilin, J. T. Devreese, C. Van Haesendonck, G. Neuttiens, *Solid State Commun*., **106**, 293 (1998).

12. L.D. Hicks, T.C. Harman, M.S. Dresselhaus, *Appl. Phys. Lett.*, 63, 3230 (1993).

13. S.S. Kubakaddi and B.G. Mulimani, *J. Appl. Phys*., **58**, 3643 (1985).

14. G. Chen and C. Tien, *J. Thermophys. Heat Transfer*, **7**, 311 (1993).

15. K.E. Goodson and Y.S. Ju, *Annu. Rev. Mater. Sci*., **29**, 261 (1999).

16. A. Balandin and K.L. Wang, *Phys. Rev. B*, **58**, 1544 (1998).

17. A. Khitun, A. Balandin and K.L.Wang, *Superlatt. and Microstruct*. **26**, 181 (1999).

18. A. Yamamoto, H. Kato, S. Kuwashiro, M. Takimoto, T. Ohta, K. Miki, K. Sakamoto, T. Matsui, K. Kamisako, in *Proceed. Of 16th Int'l Conference on Thermoelectrics*, (IEEE Cat. No. 97TH8291, ICT'97, Dresden, Germany, 1997), p. 434.

19. J.E. Parrott and A.D. Stuckes, *Thermal Conductivity of Solids*, (Methuen, Inc., New York,1975).

20. P.G. Klemens, in *Solid State Physics*, edited by F. Seitz and D. Turnbull (Academic, New York, 1958), Vol. **7**, p. 1.

21. Y.-J. Han, P.G. Klemens, *Phys. Rev. B*, **48**, 6033 (1993).

22. J. Callaway, *Phys. Rev*., **113**, 1046 (1959).

23. A. Balandin and K.L. Wang, *J. Appl. Phys.*, 84, 6149 (1998).

Alexander Balandin, *Phys. Low-Dim. Structures*., ½, 1 (2000).

24. A. Balandin and K.L. Wang, in *Nanostructures: Physics and Technology*, (Russian Academy of Sciencies, St.Petersburg, Russia, 1998), edited by Zh. Alferov *et al*., pp.24-27.

25. G.P. Srivastava, The Physics of Phonons (Adam Hilger, New York, New York, 1990), p. 175.

26. M. Wagner, *Phys. Review*, **131**, 1443 (1963).

27. N. Bannov, V. Aristov, V. Mitin, *Phys. Rev. B*, **51**, 9930 (1995).

28. A. Svizhenko, A. Balandin, S. Bandyopadhyay, M.A. Stroscio, *Phys. Rev. B*, **57**, 4687 (1998); A. Svizhenko, S. Bandyopadhyay and M. A. Stroscio, *J. Phys.: Condens. Matt.,* **11**, 3697 (1999).

29. SeGi Yu, K.W. Kim, M.A. Stroscio, G.J. Iafrate, A. Ballato, *Phys. Rev. B*, **50**, 1733 (1994).

30. G. Slack, *Phys. Rev*., **105**, 829 (1957).

31. Yonho S. Ju, K. E. Goodson, *Japanes J. Appl. Phys*., (Part 2), **36**, L798 (1997).

32. Yu. Boikov, B.M. Goltsman, V.A. Danilov, *Semiconductors*, **29**, 464 (1995).

33. J.P.Dismukes *at al.*, *J. of Appl. Phys.*, **35**, 2899 (1964).

34. S.G. Walkauskas, D.A. Broido, K. Kempa, T.L. Reinecke, *J. Appl. Phys*., **85**, 2579 (1999).

35. J. Liu, A. Balandin, T. Borca-Tasciuc, Y.S. Tang, K.L. Wang, and G. Chen, "Experimental study of phonon-folding in Si/SiGe structures designed for

thermoelectric applications," in *Proceed. of Materials Research Society*, Boston, USA, November 1998.

36. J. Heremans, C.M. Thrush, Z. Zhang, X. Sun, M.S. Dresselhaus, J.Y. Ying, D.T. Morelli, *Phys. Rev. B*, **58**, R10091 (1998).

37. N.B. Brant et. al., *Zh. Eksp. Teor. Fiz.,* **92**, 913 (1987) [*Sov. Phys. JETP*, **65**, 515 (1987)].

38. A. Balandin, S. Bandyopadhyay, P.G. Snyder, S. Stefanovich, G. Banerjee, A.E. Miller, *Phys. Low-Dim. Structur*., **11/12**, 155 (1997).

39. E. Kapon in *Optical Spectroscopy of Low Dimensional Semiconductors* Eds. G. Abstreiter, A. Aydinli and J-P Leburton, NATO ASI Series E, Vol 344 (Kluwer Academic Press, Dordrecht, 1997), pp. 99-126.

40. L.D. Hicks and M.S. Dresselhaus, *Phys. Rev. B,* **47**, 16631 (1993).

41. D.A. Broido, T.L. Reinecke, *Appl. Phys. Lett*., **67**, 100 (1995).

42. A. Casian, I. Sur, A. Sandu, H. Scherrer and S. Scherrer, in *Proceed. of the 16th International Conference on Thermoelectrics*, ICT'97, Dresden, Germany, 1997, (Piscataway, NJ, IEEE Cat. No. 97TH8291) p. 442.

43. G.D. Sanders, C.J. Stanton, Y.C. Chang, *Phys. Rev. B*, **48**, 11067 (1993).

44. H. Sakaki, *Jpn. J. Appl. Phys*., 19, L735 (1980).

45. X.F. Wang and X.L. Lei, *Phys. Rev. B*, **47**, 16612 (1993).

46. L.D. Hicks and M.S. Dresselhaus, *Phys. Rev. B,* **47**, 12727 (1993).

Alexander Balandin, *Phys. Low-Dim. Structures*., **½**, 1 (2000).

47. N. Nishiguchi, *Phys. Rev. B*, **54**, 1494 (1996).

48. A. Khitun, A. Balandin, K.L. Wang, G. Chen, "Enhancement of the thermoelectric figure of merit of SiGe quantum wires due to spatial confinement of acoustic phonons," Physica E (to appear, 1999).

FIGURE CAPTIONS

Figure 1. Scheme of the experimental sample (above) and geometry of the quantum well structure (below).

Figure 2. Dilatational acoustic phonon modes in silicon quantum well (thin film) with free-surface boundary conditions. The quantum well thickness is 10 nm. The bulk phonon dispersion is shown by dash line.

Figure 3. Shear acoustic phonon modes in silicon quantum well (thin film) with free-surface boundary conditions. The quantum well thickness is 10 nm. The bulk phonon dispersion is shown by dash line.

Figure 4. Lattice thermal conductivity of a free-standing Si quantum well and bulk. The results are also shown for thermal conductivity limited by three-phonon Umklapp process only. The quantum well thickness is 15 nm.

Figure 5. Geometry of a quantum wire and notations.

Figure 6. Acoustic phonon dispersion for longitudinal modes in Si wire of D=20 nm. The results are shown for both free-surface and clamped surface boundaries.

Figure 7. Average phonon group velocity as a function of phonon energy for Si and Ge quantum wires. The wire radius is 10 nm.

Figure 8. Phonon relaxation rates in quantum wires due to different scattering mechanisms as functions of phonon frequency at T=300 K.

Figure 9. Lattice thermal conductivity of quantum wires with free-surface and clamped surface boundaries. Note a significant drop compared to bulk.

Figure 10. Calculated electrical conductivity, thermal conductivity, Seebeck coefficient and ZT of SiGe quantum wire as functions of the wire diameter.

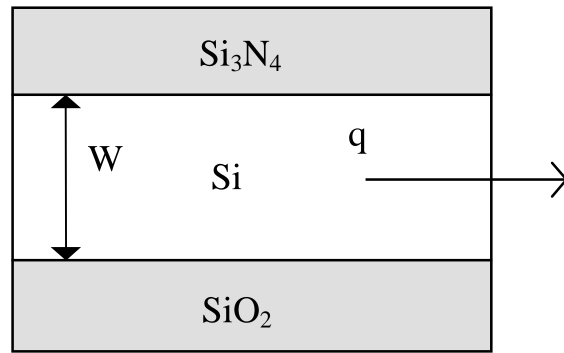
Si_3N_4
W
Si
q
SiO_2

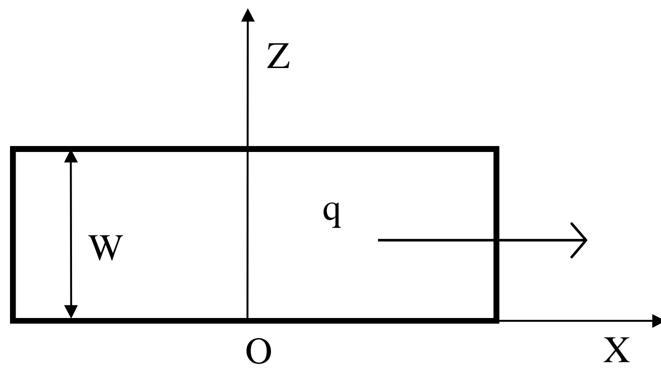
Z
q
W
O
X

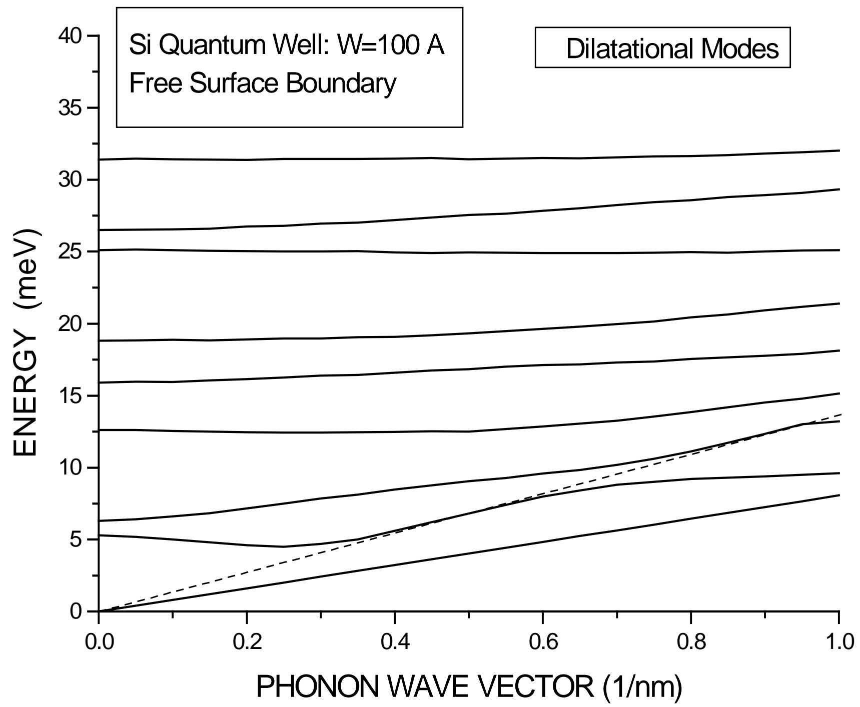
Si Quantum Well: W=100 A
Free Surface Boundary
Dilatational Modes
ENERGY (meV)
PHONON WAVE VECTOR (1/nm)
0
5
10
15
20
25
30
35
40
0.0
0.2
0.4
0.6
0.8
1.0

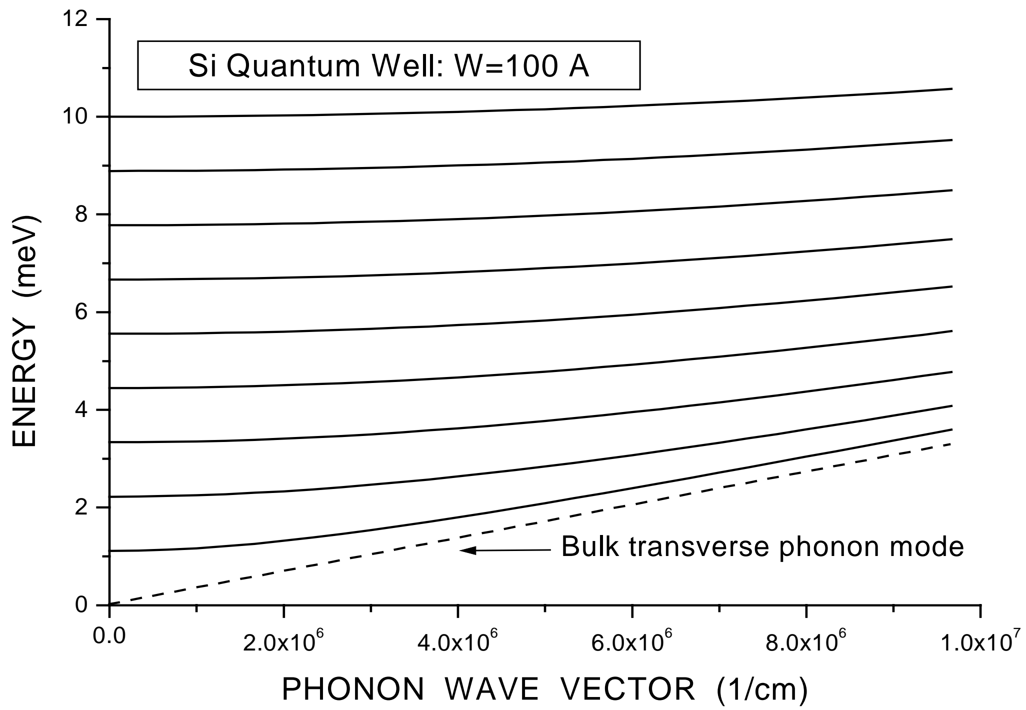
Si Quantum Well: W=100 A
ENERGY (meV)
PHONON WAVE VECTOR (1/cm)
Bulk transverse phonon mode
0
2
4
6
8
10
12
0.0
2.0x10^6
4.0x10^6
6.0x10^6
8.0x10^6
1.0x10^7

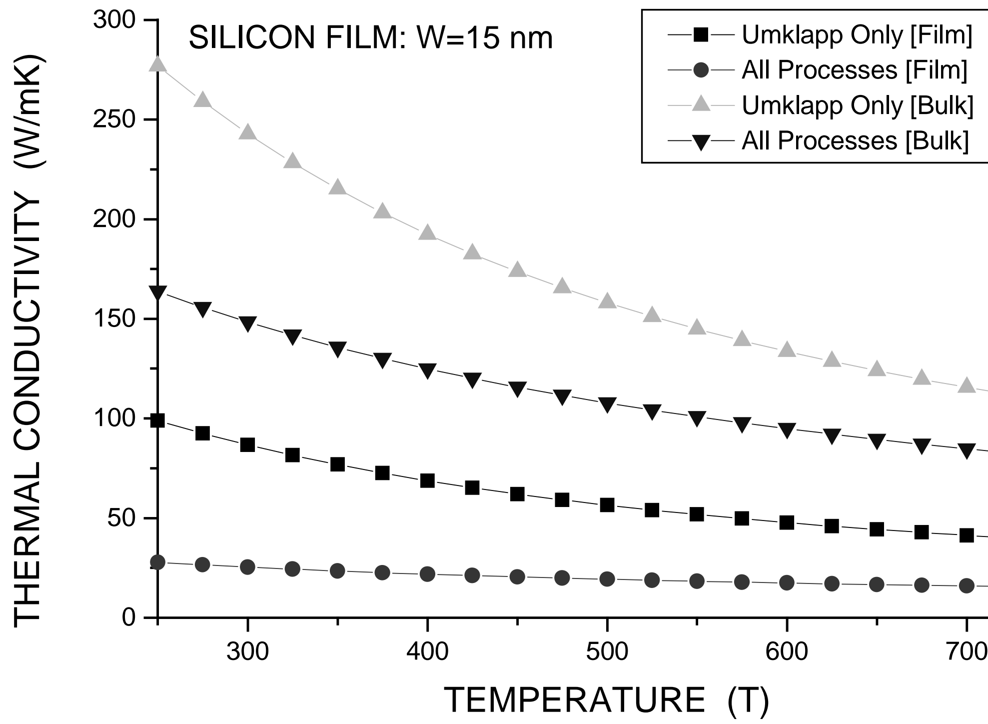
SILICON FILM: W=15 nm
Umklapp Only [Film]
All Processes [Film]
Umklapp Only [Bulk]
All Processes [Bulk]
THERMAL CONDUCTIVITY (W/mK)
TEMPERATURE (T)
0
50
100
150
200
250
300
300
400
500
600
700

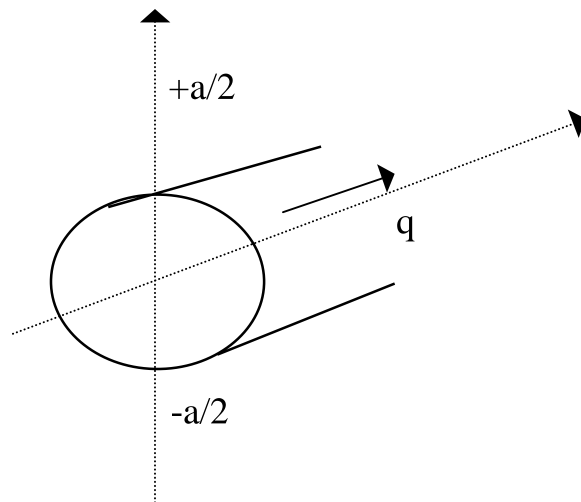
+a/2
q
-a/2

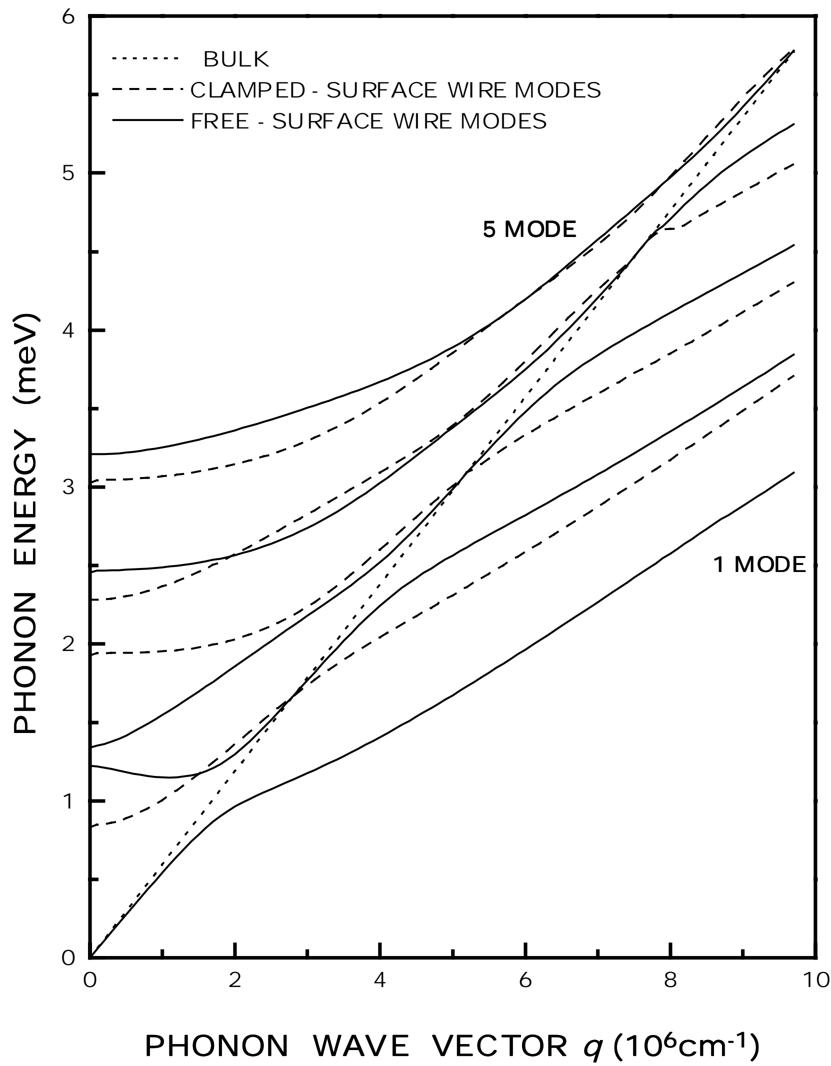
BULK
CLAMPED - SURFACE WIRE MODES
FREE - SURFACE WIRE MODES
5 MODE
1 MODE
PHONON ENERGY (meV)
PHONON WAVE VECTOR q (10⁶cm⁻¹)
0
1
2
3
4
5
6
0
2
4
6
8
10

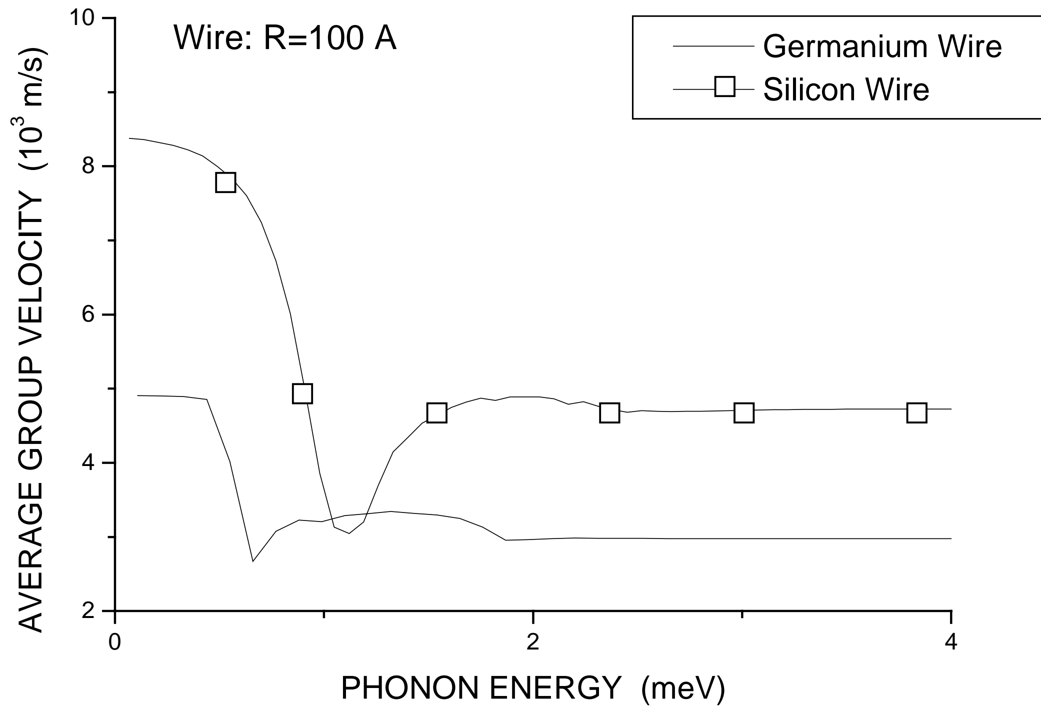
Wire: R=100 A
Germanium Wire
Silicon Wire
AVERAGE GROUP VELOCITY (10^3 m/s)
PHONON ENERGY (meV)
10
8
6
4
2
0
2
4

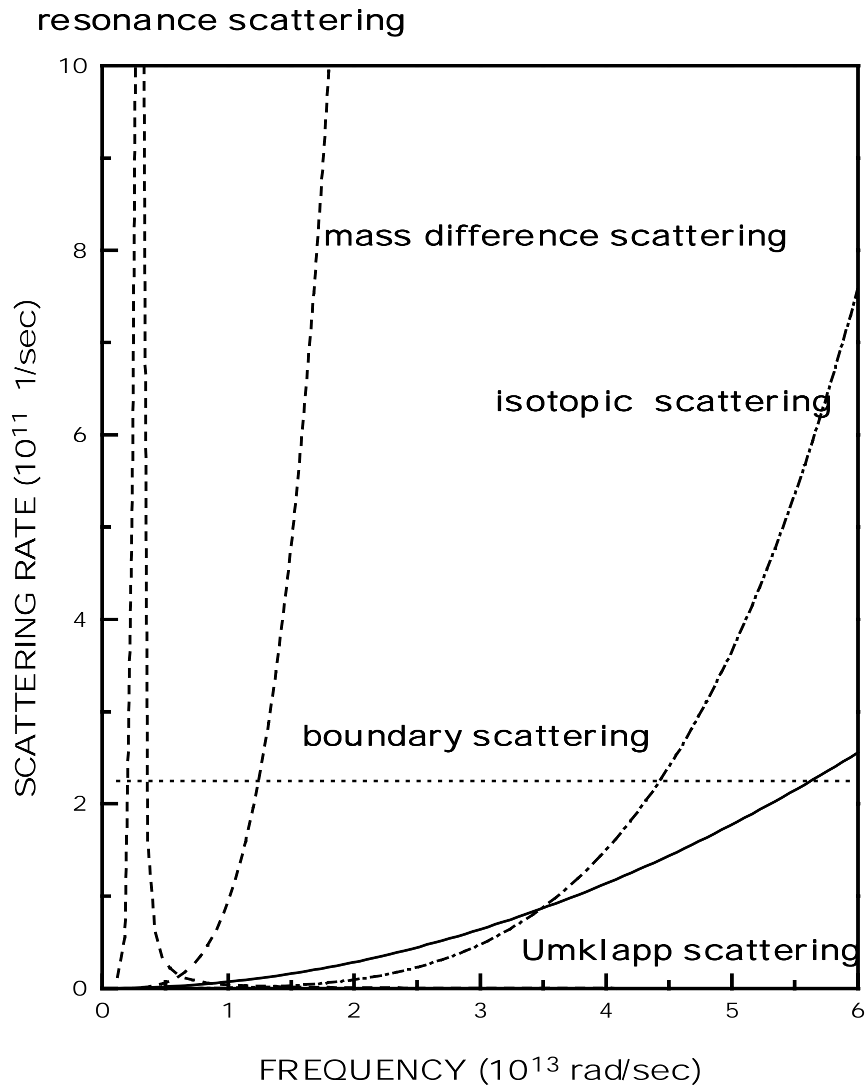
resonance scattering
mass difference scattering
isotopic scattering
boundary scattering
Umklapp scattering
SCATTERING RATE (10^11 1/sec)
FREQUENCY (10^13 rad/sec)
0
2
4
6
8
10
0
1
2
3
4
5
6

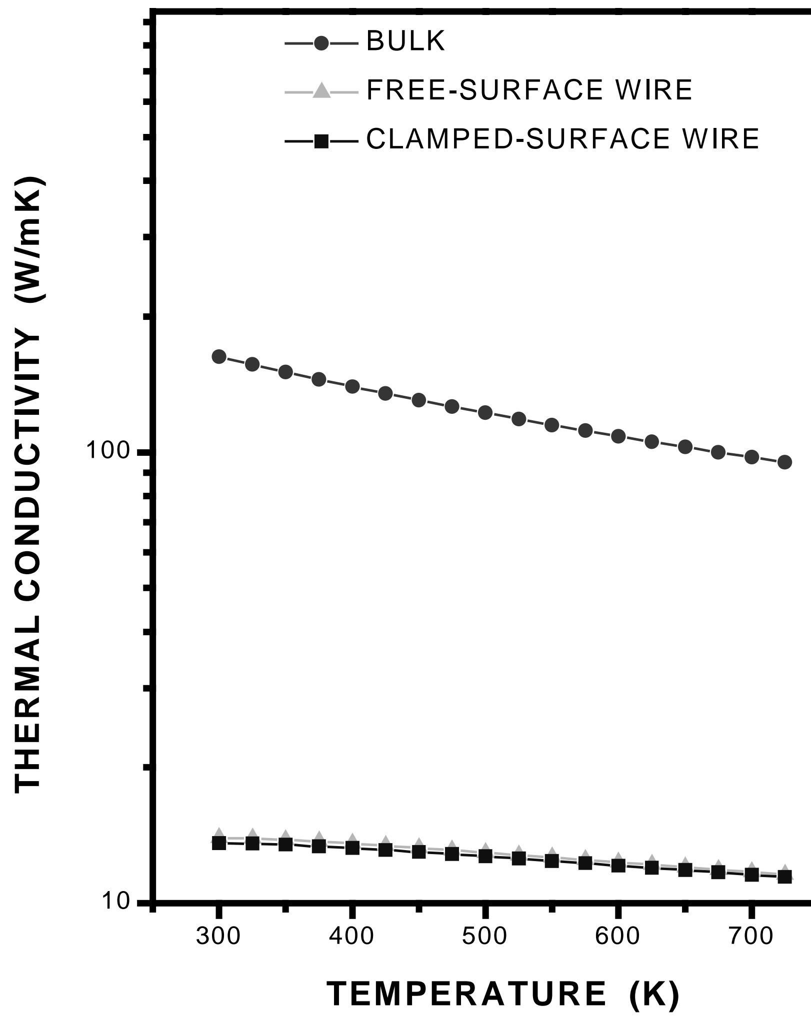
BULK
FREE-SURFACE WIRE
CLAMPED-SURFACE WIRE
THERMAL CONDUCTIVITY (W/mK)
100
10
300
400
500
600
700
TEMPERATURE (K)

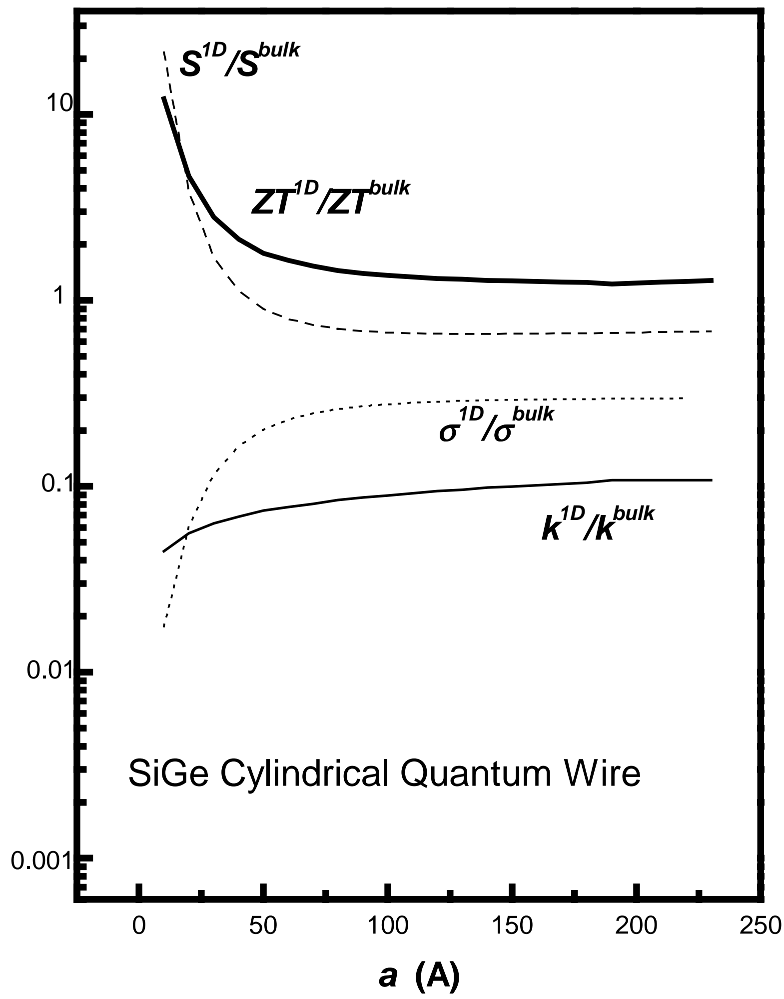

S1D/Sbulk
ZT1D/ZTbulk
σ1D/σbulk
k1D/kbulk
10
1
0.1
0.01
0.001
0
50
100
150
200
250
a (A)
SiGe Cylindrical Quantum Wire